Journal of proteome research

pubs.acs.org/jpr

Article

Glycoproteomics Identifies Plexin-B3 as a Targetable Cell Surface Protein Required for the Growth and Invasion of Triple-Negative Breast Cancer Cells

Laura Kuhlmann,[‖] Meinusha Govindarajan,[‖] Salvador Mejia-Guerrero, Vladimir Ignatchenko, Lydia Y. Liu, Barbara T. Grünwald, Jennifer Cruickshank, Hal Berman, Rama Khokha, and Thomas Kislinger*

Cite This: *J. Proteome Res.* 2022, 21, 2224−2236

Read Online

ACCESS | Metrics & More | Article Recommendations | Supporting Information

ABSTRACT: Driven by the lack of targeted therapies, triple-negative breast cancers (TNBCs) have the worst overall survival of all breast cancer subtypes. Considering that cell surface proteins are favorable drug targets and are predominantly glycosylated, glycoproteome profiling has significant potential to facilitate the identification of much-needed drug targets for TNBCs. Here, we performed *N*-glycoproteomics on six TNBCs and five normal control (NC) cell lines using hydrazide-based enrichment. Quantitative proteomics and integrative data mining led to the discovery of Plexin-B3 (PLXNB3), a previously undescribed TNBC-enriched cell surface protein. Furthermore, siRNA knockdown and CRISPR-Cas9 editing of in vitro and in vivo models show that PLXNB3 is required for TNBC cell line growth, invasion, and migration. Altogether, we provide insights into *N*-glycoproteome remodeling associated with TNBCs and functional evaluation of an extracted target, which indicate the surface protein PLXNB3 as a potential therapeutic target for TNBCs.

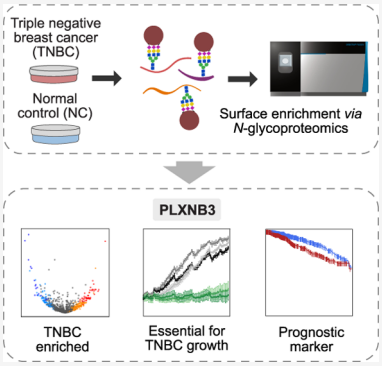

KEYWORDS: *triple-negative breast cancer, glycoproteomics, cell surface targets, spheroids, xenograft, CRISPR-Cas9*

INTRODUCTION

Triple negative breast cancers (TNBCs) are aggressive tumors defined by lack of expression of the estrogen receptor (ER), progesterone receptor (PR), and low or absent expression of human epidermal growth factor receptor 2 (HER2).[1] TNBCs are more prevalent among younger women and are associated with a higher rate of early recurrence and poorer overall survival compared to other breast cancer subtypes.[2,3] Improved therapeutic options, including the advent of therapies targeting ER+ and/or HER2+ tumors, have greatly improved the average survival of breast cancer patients. However, targeted treatment options for TNBCs remain limited, and chemotherapy and surgical tumor removal is the standard of care for most cases.[3] There is an urgent need to identify TNBC-associated proteins that can be targeted therapeutically.

Cell surface proteins represent an attractive class of molecules for targeted-therapy development, as they are easier to access by pharmaceutical compounds compared to their intracellular counterparts. Moreover, cell surface proteins can be targeted by a wide range of therapies, from small-molecule drug inhibitors (requiring a druggable domain) to immunotherapies (only requiring an extracellular epitope).[4] As a result, approximately 60% of Food and Drug Administration (FDA)-approved protein-targeting drugs are directed at cell surface proteins.[5,6]

Mass spectrometry-based proteomics is a powerful tool for detecting and quantifying novel disease-associated proteins. Cell surface proteins, however, are often underrepresented in proteomics data sets, due to their lower abundance compared to intracellular proteins and the increased hydrophobicity of their transmembrane domains, which hampers protein solubilization during analysis.[7] Thus, an in-depth analysis of the cell surface proteome (i.e., surfaceome) requires enrichment strategies.[8] Notably, >80% of cell surface proteins are predicted to be *N*-glycosylated.[9,10] Glycosylation is essential for protein function, such as cell adhesion, receptor−ligand interaction, and proper protein folding,[11] and is often enhanced or altered in cancer.[12] Moreover, *N*-glycan residues represent a useful "handle" for capturing and enriching cell surface proteins before subsequent proteomic analysis, and such enrichment protocols have been successfully used to interrogate the surfaceome of cancer cells[13−19] and normal nonmalignant cells.[20−27]

Received: June 2, 2022
Published: August 18, 2022

Here, we interrogated the *N*-glycoproteome of TNBCs and normal control (NC) cell lines using a chemical enrichment strategy, namely, *N*-glycocapture, with the goal of identifying targetable TNBC-associated cell surface glycoproteins. We employed six well-established TNBC cell lines and five nontransformed mammary epithelial cell models. This identified plexin-B3 (PLXNB3) as a novel TNBC-associated cell surface glycoprotein that has limited expression in normal tissues and, furthermore, is associated with poorer prognosis for breast cancer patients. PLXNB3 downregulation in cancer cells in vitro led to decreased cell growth in two-dimensional (2D) and three-dimensional (3D) conditions, reduced ability to grow colonies from single cells while increasing apoptosis rates, reduced migration, and partially impaired tumor growth in vivo. Therefore, PLXNB3 could represent an attractive candidate for the development of urgently needed targeted therapies in TNBCs.

EXPERIMENTAL SECTION

Data and Code Availability

Raw mass spectrometry data are publicly available from UCSD's MassIVE database (ftp://massive.ucsd.edu) with the following MassiVE ID: MSV000088911 and FTP link: ftp://massive.ucsd.edu/MSV000088911/. Processed proteomics data are available in Table S1.

Experimental Model and Subject Details

Cell Lines. All cell lines were grown at 37 °C, in 5% CO_2, 95% humidified environment. Growth media and supplements were purchased from Wisent Company unless otherwise specified. TNBC cell lines were authenticated using short tandem repeat (STR) DNA profiling identity at TCAG Facilities (Sick Kids Hospital, Toronto). All cells were tested for mycoplasma contamination using the ATCC universal mycoplasma detection kit according to the instructions of the manufacturer. TNBC cell lines were purchased from ATCC or generously provided by the Khokha lab (Princess Margaret Cancer Centre, Toronto). HCC1187 and HCC1937 were cultured according to ATCC recommendations. MDA-MB157, MDA-MB436, MDA-MB231, and MDA-MB468 cells were grown in DMEM:F12 medium supplemented with 10% fetal bovine serum (FBS) and penicillin−streptomycin−glutamine (PSG, 100 U/mL penicillin, 100 μg/mL streptomycin, 292 μg/mL L-glutamine, Gibco). MDA-MB436 growth media was supplemented with 10 μg/mL insulin. The MCF10A control cell line was purchased from ATCC and grown in DMEM:F12 media supplemented with 5% horse serum, 20 ng/mL epidermal growth factor (EGF), 10 μg/mL insulin, 500 ng/mL hydrocortisone, and 100 ng/mL cholera toxin. Four primary human mammary epithelial cell (HMEC) lines were generously provided by the lab of Dr. Hal Berman (Princess Margaret Cancer Centre, Toronto). Cells were derived from healthy women who underwent voluntary reduction mammoplasty. All patient-derived HMEC lines were confirmed to not harbor BRCA1/2 mutations. The cells were cultured using the mammary epithelial cell growth medium (MEGM) bullet kit (Lonza).

Mouse Experiments. In vivo experiments were conducted according to guidelines from the Canadian Council for Animal Care and under protocols approved by the Animal Care Committee (ACC) of the Princess Margaret Cancer Centre (AUP # 6396.3). Young adult female immunodeficient NOD/SCID/IL2Rγ -/- (NSG) mice (6−8 weeks of age) purchased from The Jackson Laboratory were used for the experiments. Mice were housed in a modified barrier, specific pathogen-free facility in sealed negative ventilation cages (Allentown) in groups of five mice per cage at 22−24 °C and a 12 h light/12 h dark cycle with food and water ad libitum.

Method Details

Unless otherwise specified, chemical reagents were purchased from Sigma-Aldrich. High-performance liquid chromatography (HPLC)-grade reagents and liquid chromatography−mass spectrometry (LC−MS) materials were purchased from Thermo Fisher Scientific.

Protein Digestion and Glycopeptide Enrichment. The glycocapture protocol was performed similarly as previously described.[28,29] Each cell line was analyzed in three processing replicates. Briefly, the cells were lysed in PBS/2,2,2-trifluoroethanol (TFE) (1:1 v/v) using five freeze−thaw cycles and pulse sonication and by incubating the lysates at 60 °C for 2 h, with vortexing every 30 min. Protein concentration was determined using the BCA assay (Pierce) according to the manufacturer's instructions, and 1 mg of the total protein was used for subsequent protein digestion and glycopeptide enrichment. Yeast invertase (SUC2) was added as an internal control at a ratio of 1 pmol of SUC2 per mg total protein. Cysteines were reduced with DTT (5 mM final concentration) at 60 °C for 30 min and subsequently alkylated using iodoacetamide (25 mM final concentration) at room temperature (RT) in the dark for 30 min. Samples were diluted 1:5 with 100 mM ammonium bicarbonate (pH 8.0) supplemented with 2 mM calcium chloride and digested overnight at 37 °C with Trypsin + LysC (Thermo) added at a 1:500 enzyme/total protein ratio. The digestion was quenched using 0.5% formic acid (FA). Tryptic peptides were desalted on C18 Macrospin columns (Nest Group), lyophilized, and resuspended in coupling buffer (0.1 M sodium acetate, 0.15 M sodium chloride, pH 5.5). Glycan chains were oxidized using 10 mM sodium metaperiodate for 30 min in the dark and peptides were again desalted and lyophilized on C18 Macrospin columns. Peptides were resolubilized in coupling buffer and oxidized glycopeptides were captured on hydrazide magnetic beads (Chemicell, SiMAG Hydrazide) for 12 h at RT. The coupling reaction was catalyzed by adding aniline (50 mM final concentration) and the reaction continued for three additional hours at RT. Glycopeptides covalently bound to the hydrazide beads were thoroughly washed (2 × coupling buffer; 5 M × 1.5 M sodium chloride; 5 × HPLC-grade water; 5 × methanol; 5 × 80% acetonitrile; 3 × water; 3 × 100 mM ammonium bicarbonate, pH 8.0) to remove nonspecific binders. *N*-Glycopeptides were enzymatically deglycosylated and eluted using 5 U PNGase F (Thermo) in 100 mM ammonium bicarbonate at 37 °C overnight. Eluted deglycosylated peptides were recovered, and the hydrazide beads were additionally washed twice with an 80% acetonitrile solution. Deglycosylated peptides were desalted using C18 stage tips (3M Empore), eluted using 80% acetonitrile with 0.1% F.A., and lyophilized. The purified deglycosylated peptides were dissolved in 21 μL of 3% acetonitrile with 0.1% F.A.

Mass Spectrometry-Based Proteomics. The peptide concentration was determined using a NanoDrop 2000 (Thermo) spectrophotometer, and 1.5 μg of formerly glycosylated peptides were loaded on a 50 cm ES803 column (Thermo). Peptides were separated using a 2 h gradient, at 250 nL/min flow, using a thermo scientific easyLC1000 nano-liquid chromatography system. The chromatography system was coupled to an orbitrap fusion mass spectrometer (Thermo).

https://doi.org/10.1021/acs.jproteome.2c00332
J. Proteome Res. 2022, 21, 2224−2236

MS1 profiles were acquired on the Orbitrap detector, with a scan range of 250−1550 (m/z) and at a resolution of 120 000; MS/MS data were acquired in a top-speed data-dependent mode on an orbitrap mass detector at a resolution of 15 000, and the maximum injection time was set to 100 ms. The acquired raw data were analyzed using MaxQuant software (version 1.5.8.3) using the complete human proteome (version 2016.07.13 containing 42 041 sequences). Proteins were detected with a minimum of one razor peptide, and match-between-runs was enabled. Search parameters were defined as follows: a maximum of two missed cleavages; carbamidomethylation of cysteine was specified as fixed modification; oxidation of methionine and deamidation of asparagine to aspartic acid (as a result of the PNGase F elution) were specified as variable modifications. The fragment ion peptide tolerance was ±20 ppm, and the parent ion mass tolerance was ±10 ppm. The false discovery of peptides was controlled using a target-decoy approach based on reversed sequences,[30] and the false discovery rate was defined as 1% at site, peptide, and protein levels.

Data Analysis and Protein Quantification. The PNGase F cleavage of glycan chains bound to asparagine residues results in the conversion of asparagine to aspartic acid. Bioinformatic analysis was performed on the MaxQuant output file: AsnAspSites.txt using R (version 3.6.2). Only asparagine deamidation events identified with a localization probability of minimum 0.8, which were also part of the *N*-glycosylation N-[!P]-STC sequon (N = asparagine; [!P] = any amino acid other than proline; STC = serine, threonine, or cysteine at the +2 site), were carried forward for analysis. For each analyzed cell line, peptides that were detected in only one out of the three processing replicates were excluded. Peptide intensities were $\log_2$ transformed and normalized against the average intensity of three SUC2 peptides detected in all samples: AEPILNISNAGPWSR, FATNTTLTK, and NPVLAANSTQFRDPK. Missing values for the peptides that were quantified in two out of three replicates of the same sample were imputed with the average value of the other two replicates. In cases where the peptide was not quantified or quantified in only one of the three replicates of the same sample, a small random value between 1 and 1.1 $\log_2$ intensity was imputed instead. Protein intensities were calculated by averaging the respective peptide intensities. For visualizing protein intensities, proteins were ordered based on mean $\log_2$ intensity across all samples, and the protein with the highest mean $\log_2$ intensity was given rank 1.

Data Mining and Candidate Selection. Hierarchical clustering of the samples was performed using Spearman's rank correlation, and heatmaps were generated using ComplexHeatmap package version 2.4.3. Protein subcellular localization annotations were based on UniProt keywords. PCA analysis was performed based on centered and scaled protein intensities, using the stats R package (version 3.6.2). For differential expression analysis between TNBC and NC, a fold change was calculated based on averaged protein intensities for each condition and student's *t*-test followed by a Benjamini−Hochberg correction was used. The quantified data set was searched against the bioinformatics tool SurfaceGenie[31] to identify cell surface proteins with high confidence. Normal tissue expression was evaluated by downloading normal tissue protein staining data from the Human Protein Atlas[32] version 20.1. The proportion of "high", "medium", "low", and "not detected" as well as NA annotations across all tissues were calculated for each shortlisted protein and plotted in R using ggplot2.

To select candidates for functional evaluation, we considered glycoproteins with a $\log_2$ protein fold change in TNBC versus NC samples > 2 and an adjusted p-value < 0.05. We further restricted candidates to high-confidence cell surface proteins, denoted by a surface prediction consensus (SPC) score > 1, and those that were detected in at least four TNBC cell lines more than the number of positive NC lines (i.e., the number of TNBC cell lines minus the number of NC cell lines a protein was detected in ≥4; e.g., a protein had to be detected in four TNBC cell lines and zero NC cell lines or a protein had to be detected in five TNBC cell lines and a maximum of one NC cell line to pass this threshold). Glycoproteins that passed these filters were ranked based proportion of normal tissues that a protein was not detected within the Human Protein Atlas database to prioritize candidates with limited overall expression in normal tissue. In addition, we used global proteomics data from the GTEx Consortium[33] to further evaluate candidate expression in normal tissues using $\log_2$ normalized protein abundance values available in tables given in the Supporting Information.

Gene Ontology Analysis. Functional enrichment of differentially expressed proteins was performed using g:Profiler,[34] and data visualization was completed in R using ggplot2. TNBC-enriched glycoproteins were proteins with the $\log_2$ protein fold change in TNBC versus NC samples > 2 and an adjusted p-value < 0.05; NC-enriched glycoproteins were proteins with the $\log_2$ protein fold change in TNBC versus NC samples <−2 and an adjusted p-value < 0.05.

PLXNB3 Survival Analysis in Breast Cancer. PLXNB3 survival analysis was performed using the mRNA expression and overall survival data in the full breast cancer cohort from TCGA[35] (n = 1079) and in TNBC patients (defined as negative ER, PR, and HER2) from the METABRIC data set[36] (n = 299). Median PLXNB3 mRNA expression was used to define high and low expressions. A log-rank test was used to test statistical significance, and data visualization was performed using the BPG framework[37] in R (version 3.6.2).

siRNA Transfection. A reverse-transfection protocol was employed for transient downregulation of targets of interest. Lipofectamine RNAiMAX Transfection Reagent (Thermo) scrambled (Scr control) and PLXNB3 siRNAs (27mer siRNA duplexes, Origene, SR303587; siA: GUACUAUGAUCAGAUUAUCAGUGCC; siB: GAGCUCUCCGGGAACUACACUUCTG) were preincubated separately at RT for 5 min in Opti-MEM (Gibco). RNAiMAX was then combined with the siRNAs and incubated for an additional 20 min at RT. The mixture was added to the growth plates (20 μL for 96-well plates; 500 μL for 6-well plates). The cells were counted and plated on top of the agent-RNA mixture (4×10^3 cells for 96-well plates; $(3-4) \times 10^5$ cells for 6-well plates). The culture medium was refreshed after 24 h following cell adhesion. Mock (transfection reagent only) and nontreated (NT) controls were included in all experiments. The siRNA-induced PLXNB3 downregulation was stable for up to five days (data not shown).

CRISPR Downregulation. Generation of sgRNA-Cas9 coexpressing vectors was performed as previously described.[38] Briefly, sgRNAs were cloned into the pSpCas9(BB)-2A-Puro (PX459) V2.0 (Adgene) vector, containing a functional puromycin cassette and Cas9. sgRNAs targeting PLXNB3 were selected from the Toronto KnockOut Library V3 (TKOv3):[39] sg1: AGGCCAGCGAGCCATCACGG; sg2: GCACATGATAGCCTTCCTGG. The selected control guide RNA was sgRNA GFP: GGCGAGGAGCTGTTCACCG.[40] sgRNA oligos (top and bottom) were ordered from Origene.

https://doi.org/10.1021/acs.jproteome.2c00332
J. Proteome Res. 2022, 21, 2224−2236

Each pair was phosphorylated using T4 polynucleotide kinase in the T4 DNA ligase reaction buffer, 10× (both New England Biolabs). The phosphorylated and annealed oligos were diluted 1:200 and cloned into the pSpCas9(BB)-2A-Puro (PX459) V2.0 vector using FastDigest *Bbs*I (BpiI) nuclease (Thermo) and T7 DNA ligase (New England Biolabs). The ligation reaction was incubated for a total of ∼80 min as follows: six cycles at 37 °C/8 min digestion, followed by 21 °C/5 min ligation. The ligation reaction was subsequently incubated with PlasmidSafe ATP-dependent DNase (Lucigen) at 37 °C for 30 min, followed by 70 °C for 30 min to digest any residual linear DNA. The PlasmidSafe-treated plasmid was transformed into *Stbl3* chemically competent *Escherichia coli* (Life Sciences), using the heat shock method according to the protocol of the manufacturer. Bacteria were plated onto an LB plate containing 100 μg/mL ampicillin and incubated overnight (∼16 h) at 37 °C. Plasmid DNA was isolated from transformed colonies using a QIAprep spin miniprep kit (QIAGEN) according to the manufacturer's instructions. The sgRNA sequence and insertion site were verified by Sanger Sequencing (TCAG Facilities, Sick Kids Hospital, Toronto). MDA-MB468 cells were reverse-transfected in antibiotic-free media with 500 ng of vector per 2×10^5 cells using the X-tremeGENE HF reagent (Sigma). For puromycin selection, MDA-MB468 cells were cultured in PSG-free, 2 μg/mL puromycin-containing growth media for 48 h. Subsequent experiments were performed using polyclonal populations. PLXNB3 downregulation was verified by western blotting (WB) and qPCR. pSpCas9(BB)-2A-Puro (PX459) V2.0 with no sgRNA controls (Cas9 controls) were included in all experiments.

Proliferation Assays. For proliferation assays, 4×10^3 cells (MDA-MB157, MDA-MB436; MDA-MB468; HCC1937; MCF10A) were seeded in 96-well plates and allowed to adhere overnight. Cell confluency was monitored using an IncuCyte ZOOM System (Essen BioScience). Cell proliferation was quantified using the metric Phase Object Confluence (POC), a measure of the area of field of view covered by cells. Mean POC percentages and standard deviations of three to six replicates were plotted using R (version 4.1.2). Statistical analysis was performed on POC measurements at the final time point using a one-way ANOVA followed by Tukey's multiple comparison test to assess differences against the scrambled or GFP control in siRNA or CRISPR experiments.

Spheroid Assays. To evaluate 3D cell growth following PLXNB3 downregulation, $(5-6) \times 10^3$ cells (MDA-MB157, MDA-MB468, HCC1937) were seeded in poly-HEMA-coated round-bottom 96-well plates. For transient downregulation conditions, cells were reverse-transfected on 6-well plates for 24 h, then detached, and counted. Spheroids were allowed to form for 24−48 h, after which half of the wells were embedded with 30 μL of Matrigel (Corning). Spheroid growth was monitored every 48 h on a Leica DMi1, equipped with an MC170 HD camera microscope. Each experiment was performed in triplicates and was repeated twice. The number of Matrigel-invading cancer cells was quantified using ImageJ (version 1.53.e) using the "analyze particles" function. For this purpose, pictures were converted to 8-bit, contrast was adjusted identically for all pictures, and particles between 200−2000 pixels, with a circularity between 0 and 1, were counted. Means and the number of invaded cells in individual replicates were plotted using R (version 4.1.2). A one-way ANOVA followed by Tukey's multiple comparison test was used to assess statistical differences in invasion against the scrambled control.

Colony Forming Assays (CFA). Following PLXNB3 knockdown (KD) using 5 nM siRNA, cells (MDA-MB157, MDA-MB436, HCC1937) were counted and seeded in 6-well plates at a density of 500 cells/well. Cells were allowed to grow undisturbed for 14−21 days, after which they were fixed with cold methanol for 20 min at RT and stained with 0.01% crystal violet in dH_2O containing 10% methanol for 1−2 h at RT. Colony counting was performed using ImageJ. Briefly, the area of interest was defined for each well, excluding the well's edge. Images were converted to 8-bit grayscale, and the threshold was adjusted identically for all images in one experiment until all colonies were visualized clearly. We next performed watershed segmentation to avoid undercounting adjacent colonies. Finally, the colonies were counted using the analyze particles function, and the data were exported as.csv for statistical analysis.

Cell Migration Assays. PLXNB3 was downregulated using 5 nM siRNA and the cells were detached with trypsin and thoroughly counted. An optimal number of cells (20 000 for MDA-MB157; 80 000 for MDA-MB436; 40 000 for HCC1937) was seeded in 300 μL of serum-free media on top of 24 plate Transwell inserts (0.33 cm^2 area; 6.5 mm PC membrane thickness; 0.8 μm pore size; VWR). The inserts were transferred in 24-well plates into wells containing a growth medium with 10% FBS and were cultured for 18 h at 37 °C. Migrated cells were fixed using ice-cold methanol for 10 min and stained with 0.01% crystal violet in dH_2O containing 10% methanol for 1−2 h at RT. Nonmigrated cells on top of the well were removed using a cotton swab. Pictures were taken using an upright microscope and the number of migrated cells was quantified in ImageJ (version 1.53.e) using the analyze particles function, as previously described (see the Spheroid Assays section). Means and the number of migrated cells in individual replicates ($n = 3$) were plotted using R (version 4.1.2). Statistical analysis was performed using a one-way ANOVA followed by Tukey's multiple comparison test against the scrambled control.

Western Blot Analysis. Whole cell lysates were prepared using RIPA buffer (50 mM Tris-HCl pH 8, 150 mM NaCl, 5 mM EDTA, 1% NP-40, 0.1% SDS), supplemented with Pierce protease inhibitor tablets and Pierce phosphatase inhibitor mini tablets (Thermo). For western blotting, 15−30 μg of the total protein was resolved on 8−15% freshly poured SDS-PAGE and blotted on PVDF membranes (0.2 μm; Bio-Rad). The membranes were blocked for 1 h in 5% milk-TBS containing 0.1% (v/v) Tween-20. Primary antibodies were incubated O/N at 4 °C in a blocking solution. Secondary HRP-coupled antibodies were diluted 1:2000 in the blocking solution and incubated for 1 h at RT. Membranes were washed in 0.1% TBS-Tween, and immunocomplexes were detected using the SuperSignal West Femto Maximum Sensitivity chemiluminescent substrate (Thermo). Bands were detected using a MicroChemi chemiluminescence image analysis system (DNR Bioimaging Systems). The antibodies used for western blotting experiments are listed in Table 1. M.C. = monoclonal. P.C. = polyclonal.

In Vivo Tumor Growth Experiment. For in vivo experiments, 1×10^6 MDA-MB468 cells were resuspended in 100 μL of equal volume growth factor reduced Matrigel (Corning) and DMEM:F12 media and injected subcutaneously into the right flank of each animal. Five animals were injected per condition (two CRISPR polyclonal populations and three controls, including sgGFP, Cas9, and nontreated controls). Tumors were measured biweekly using calipers, and tumor volume (V) was calculated with the formula $V = 0.5 \times l \times w^2$,

https://doi.org/10.1021/acs.jproteome.2c00332
J. Proteome Res. 2022, 21, 2224−2236

Table 1. List of Antibodies Used for Western Blotting Experiments

target	species	clonality	company	ordering number	dilution
PLXNB3	sheep	P.C.	novus	AF4598	1 μg/mL
LAMB1	rabbit	M.C.; clone D4Q4Z	cell signaling	12 586	1:1000
cleaved-CASP3	rabbit	M.C.; clone 8G10	cell signaling	9665	1:1000
CASP3	rabbit	P.C.	cell signaling	9661	1:1000
cleaved-CASP7	rabbit	M.C.; clone D6H1	cell signaling	8438	1:1000
CASP7	rabbit	M.C.; clone D2Q3L	cell signaling	12 827	1:1000
anti-sheep	donkey	P.C.	santa cruz	SC2473	1:5000
anti-mouse	horse	P.C.	cell signaling	7076P2	1:2000
anti-rabbit	goat	P.C.	cell signaling	7074	1:2000

where l and w are the longest and shortest perpendicular measurements, respectively. As recommended by the ACC, the endpoint was defined as when the nontreated MDA-MB468 (parental) xenografts reached approximately 15 mm in length. At the endpoint, the animals were sacrificed with CO_2 and tumors were removed, measured, and weighed. Tumor volume and tumor weight measurements were plotted using R (version 4.1.2). A one-way ANOVA followed by Tukey's multiple comparison test was used to assess differences in tumor volumes and weights at the endpoint against the sgGFP control.

Quantification and Statistical Analysis

Specific quantitative analyses and statistical tests are indicated in figure legends and/or the appropriat Methods section section and were performed within the R statistical environment. Statistical significance was set at $p < 0.05$. Data were visualized using R packages ggplot2, BPG, and ComplexHeatMap or using GraphPad, as indicated in the appropriate Methods section.

RESULTS AND DISCUSSION

Interrogating the *N*-Glycoproteome of Triple-Negative Breast Cancer and Normal Mammary Epithelial Cells

To comprehensively analyze the *N*-glycoproteome of TNBC and compare it to normal mammary epithelial cells, we applied an *N*-glycocapture protocol[29,41] (Figure 1A) to a cohort of six commercially available TNBC cell lines (HCC1187, HCC1937,

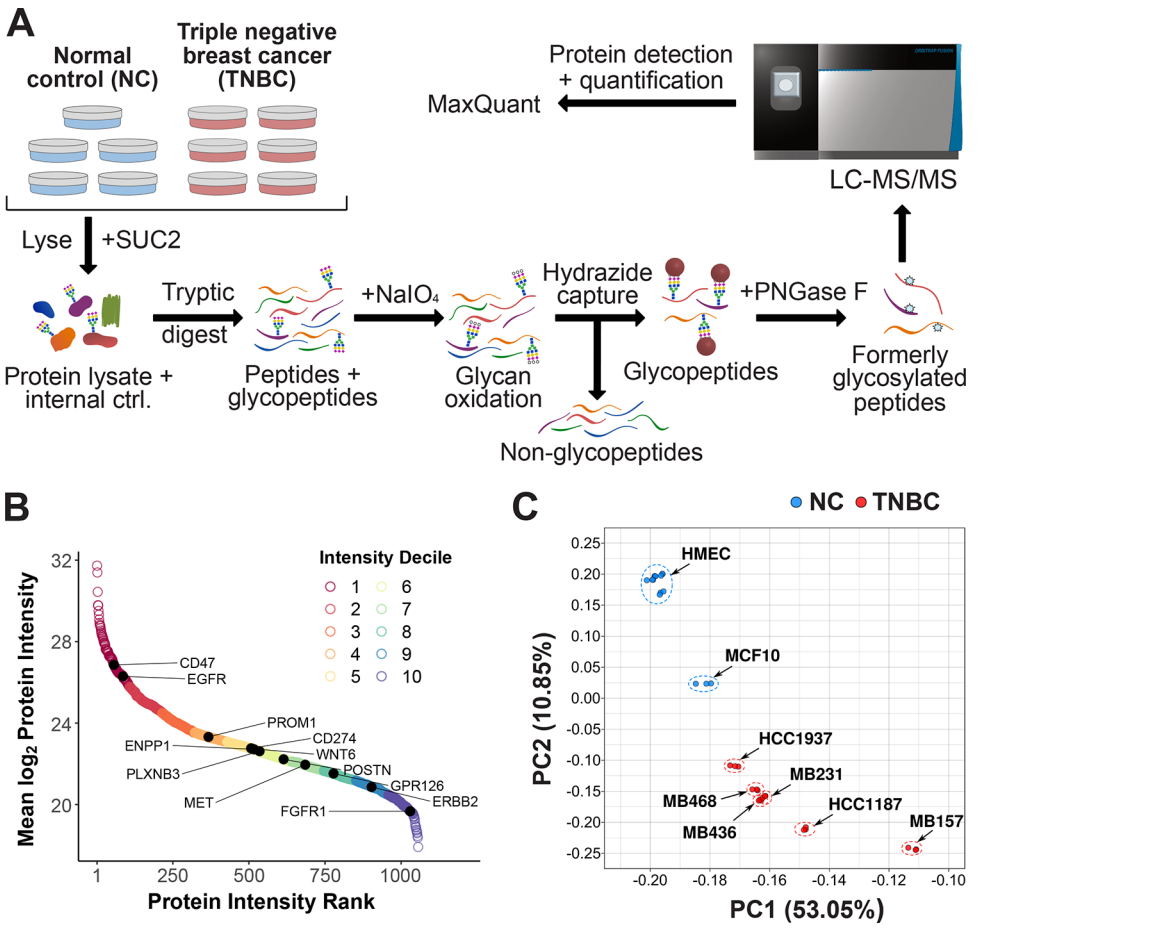

Figure 1. *N*-glycoproteome of triple negative-breast cancer and normal controls. (A) *N*-glycoproteomics workflow. Six triple-negative breast cancer (TNBC) and five normal mammary epithelial control (NC) cell lines were analyzed in three processing replicates using a chemical proteomics enrichment protocol. (B) Rank intensity plot showing intensity distributions of the detected glycoproteins. Average protein intensity was calculated based on nonimputed values, and proteins were ranked from highest to lowest intensity. Color represents intensity deciles (highest to lowest). Previously described breast cancer cell surface proteins are indicated in the figure. (C) Principal component analysis (PCA) of the TNBC ($n = 6$) and NC ($n = 5$) *N*-glycoproteome. Each dot represents a processing replicate and dashed ellipses delineate processing replicates of the same cell line. See also Figure S1.

https://doi.org/10.1021/acs.jproteome.2c00332
J. Proteome Res. 2022, 21, 2224−2236

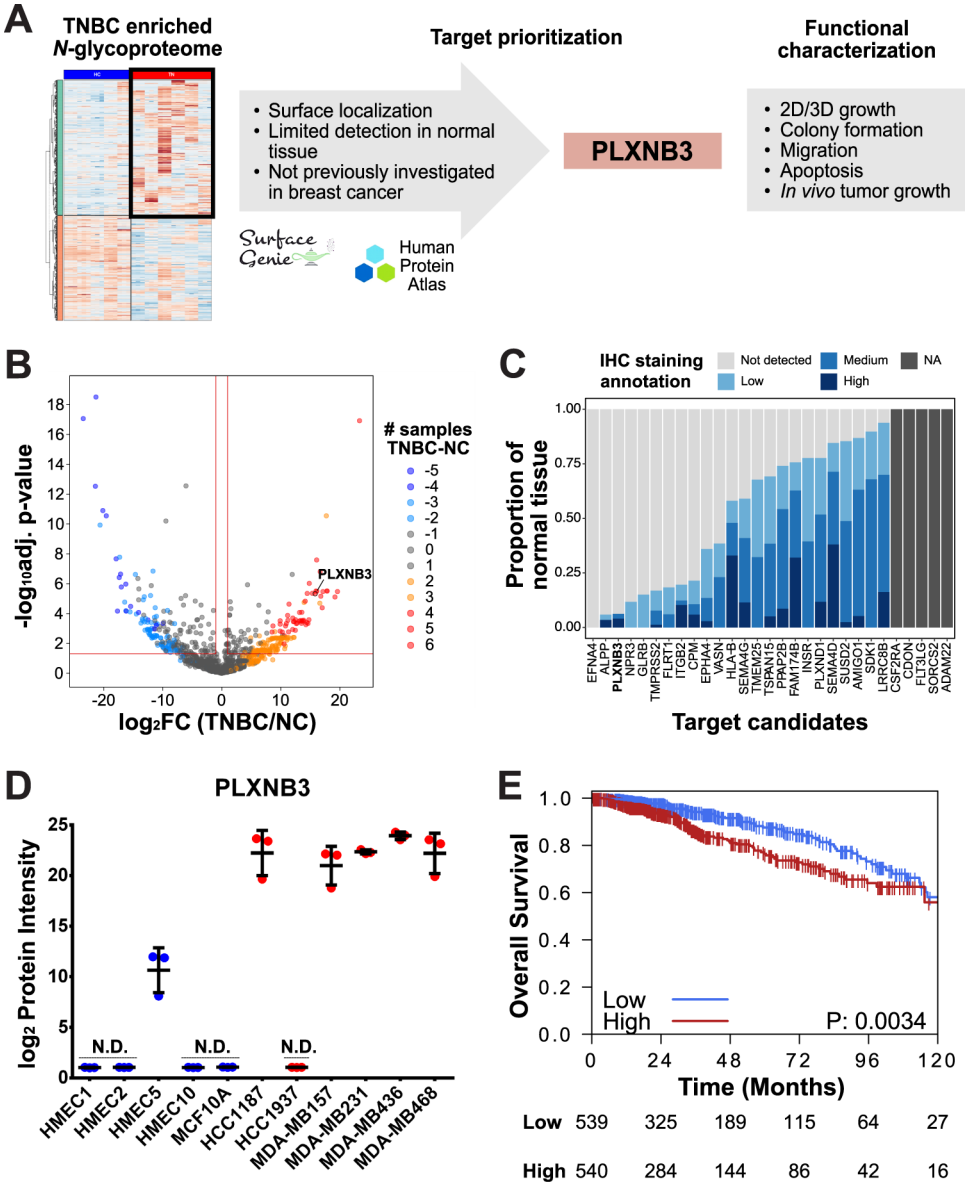

Figure 2. Identification of PLXNB3 as a novel TNBC-associated surface protein. (A) Data mining and functional characterization workflow. The list of TNBC-enriched *N*-glycoproteins was restricted to include only cell surface proteins[31] and was subsequently ranked based on the lack of detection in normal tissue according to the Human Protein Atlas.[32] PLXNB3 was the top-ranking candidate that had not previously been investigated in the context of breast cancer and hence was selected for functional interrogation. (B) Volcano plot highlighting differentially expressed TNBC and NC proteins. Cutoff values (red dotted lines): $\log_2$ fold change > 2 (vertical) and adjusted *p*-value < 0.05 (horizontal). The color of dots represents the number of TNBC cell lines positive for a respective protein and minus the number of positive NC cell lines. Intense red signifies proteins detected exclusively in TNBC samples, whereas intense blue signifies proteins exclusively detected in NC cells. (C) TNBC-enriched cell surface proteins ranked based on the lack of immunohistochemistry (IHC) detection in normal tissue. The proportion of normal tissue with high, medium, low, not detected, and NA IHC staining annotations was calculated from the Human Protein Atlas (version 20.1) data. (D) PLXNB3 expression levels in the analyzed cell lines as determined using the glycoproteomics method. N.D. = not detected. (E) Overall survival of breast cancer patients (n = 1079) based on PLXNB3 mRNA expression levels.[35] Median PLXNB3 mRNA expression levels were used as the cutoff for high and low expressions. See also Figure S2.

MDA-MB157, MDA-MB231, MDA-MB436, and MDA-MB468) and five NC samples (the immortalized cell line MCF10A and four nonimmortalized HMECs) derived from healthy patients undergoing voluntary reduction mammoplasty (Figure S1A). Three processing replicates were analyzed per cell line. The *N*-glycocapture protocol led to the detection of 2855 deamidated sites with high-confidence site localization (localization probability > 0.8). Consistent with prior publications,[29] more than 79% of deamidations were part of the *N*-glycosylation sequon (N-[!P]-STC). To further restrict our list to high-confidence events, we retained only those deamidation events detected in at least two processing replicates per cell line. The filtered list included 2242 deamidation events, mapping to 2149 peptides and 1044 protein groups (Table S1), including several detected proteins that have previously been linked to breast cancer pathogenesis, including epidermal growth factor receptor (EGFR), hepatocyte growth factor receptor (MET), fibroblast growth factor receptor 1 (FGFR1), and receptor tyrosine-protein kinase erbB-2 (ERBB2) to name a few (Figure 1B).[1,42−47] To our knowledge, the current study represents the most in-depth analysis of the TNBC *N*-glycoproteome.

https://doi.org/10.1021/acs.jproteome.2c00332
J. Proteome Res. 2022, 21, 2224−2236

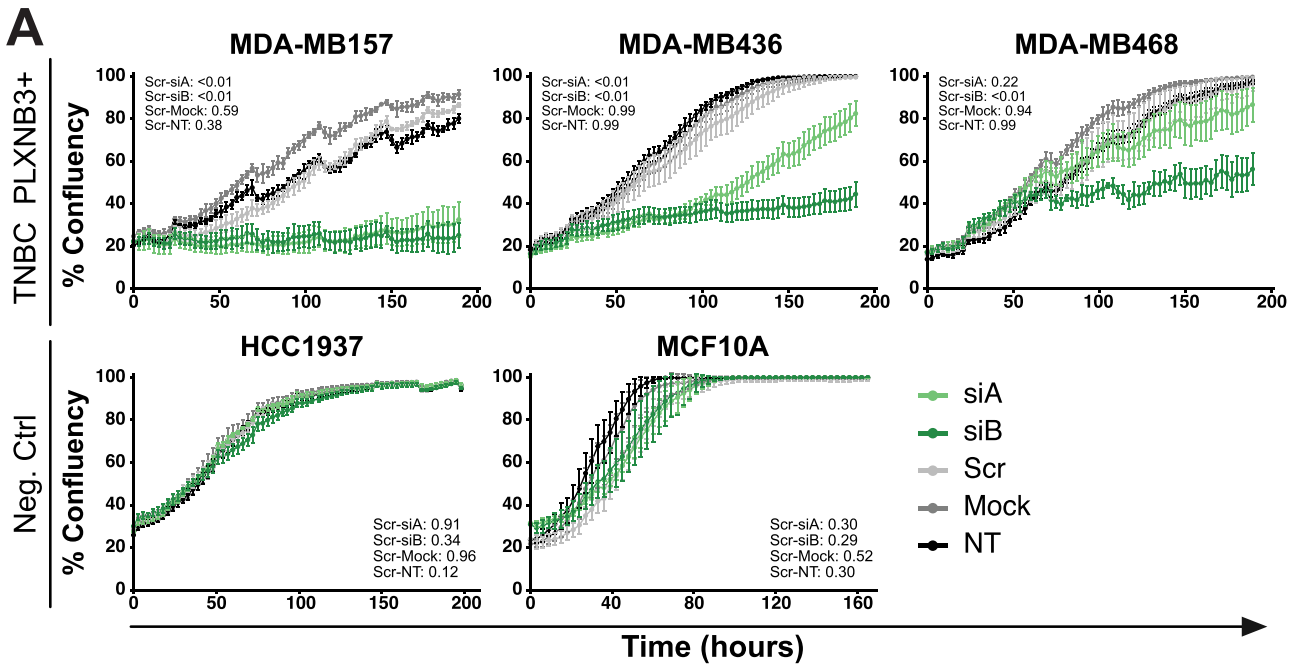

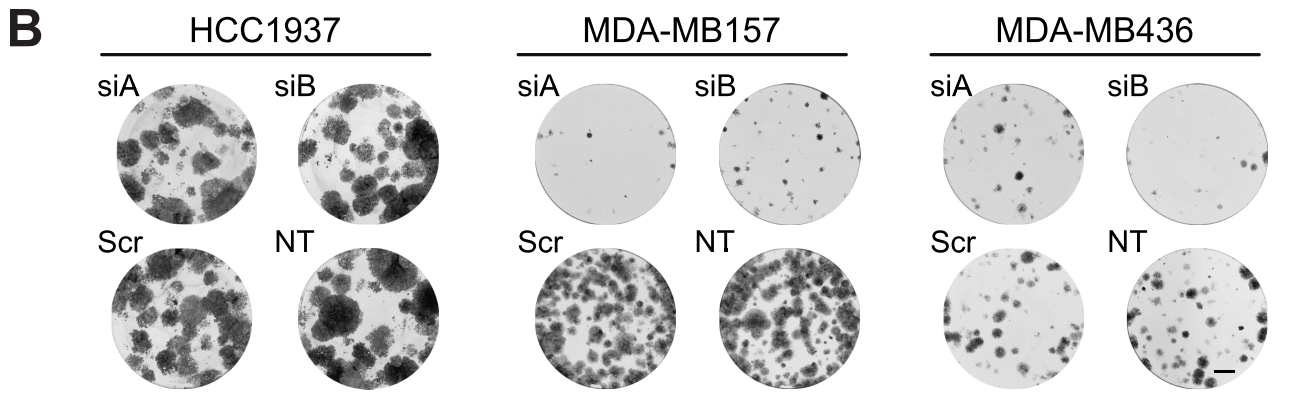

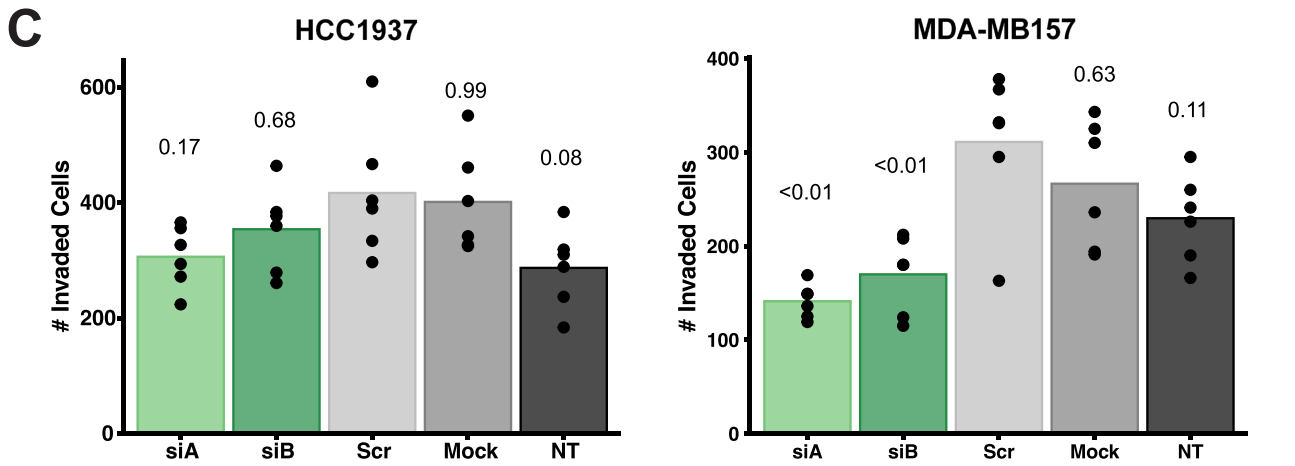

Figure 3. siRNA-mediated knockdown of PLXNB3 negatively impacts TNBC growth and invasion in vitro. (A) PLXNB3 KD using 5 nM siRNA negatively impacts the 2D cell growth of PLXNB3-positive cells, as determined using the growth curve assay. The PLXNB3-negative TNBC cell line HCC1937 and the control cell line MCF10A were used as negative controls. Average values with standard deviation are represented ($n = 3$). *P*-values from Tukey's multiple comparisons test against Scr control are reported. NT = nontreated cells. (B) PLXNB3 KD (5 nM siRNA) negatively impacts TNBC cell ability to undergo unlimited cell divisions as determined using the colony forming assay. The PLXNB3-negative cell line (HCC1937) was used as a negative control. Scale bar = 5 mm. (C) PLXNB3 KD (5 nM siRNA) negatively impacts TNBC cell ability to invade Matrigel as determined using the 3D spheroid growth assay ($n = 6$). The number of invading cells was determined using ImageJ. *P*-values from Tukey's multiple comparisons test against Scr control are reported. See also Figure S3.

https://doi.org/10.1021/acs.jproteome.2c00332
J. Proteome Res. 2022, 21, 2224−2236

Seven hundred and thirty-one of the detected proteins (>70%) were predicted to be localized at the plasma membrane by SurfaceGenie.[31] Peptide intensities were log-transformed and normalized based on the average SUC2 peptide intensities across all samples; protein intensity was calculated based on averaged peptide intensity. Principal component analysis (PCA) was performed to analyze the degree of similarity between samples (Figure 1C): the NC samples clustered apart from TNBC cell lines with all nonimmortalized HMEC cell lines and replicates clustering tightly together; a high degree of variability was detected among TNBC cell lines.

The 1044 detected glycoproteins clustered based on expression differences in TNBC (right) and NC (left, Figure S1B). We could once again confirm the preponderance of the cell surface and secreted proteins based on UniProt keywords. We subsequently performed gene ontology (GO) and KEGG analysis on differentially expressed proteins using g:profiler.[34] Selected biological process (BP) GO terms unique to TNBC samples (Figure S1C) included: transmembrane receptor tyrosine kinase signaling, regulation of neuron projection development, MAPK, and PKB signaling, and semaphorin-plexin signaling pathway (Table S2). In contrast, proteins enriched in the normal controls mapped to GO-BP terms such as cell-matrix adhesion, cell junction organization, angiogenesis, and wound healing (Figure S1D and Table S2). KEGG annotations unique to the TNBC-enriched subproteome (Figure S1E) included: axon guidance, MAPK signaling pathway, and complement and coagulation cascades. In contrast, KEGG annotations unique to the NC-enriched subproteome (Figure S1F) included: cell adhesion molecules and several cardiomyopathy functional annotations. PI3K-AKT signaling, focal adhesion, and ECM-receptor interaction KEGG annotations were common for both TNBC-enriched and NC-enriched glycoproteomes.

Integrative Data Mining Identifies PLXNB3 as a Novel TNBC-Associated Protein

To identify novel TNBC-associated proteins, we integrated our TNBC *N*-glycoproteomics data with publicly available resources (Figure 2A). Specifically, we filtered for proteins that were enriched in TNBC compared to NCs (Figure 2B) and were predicted to have a cell surface localization by SurfaceGenie.[31] We next ranked the shortlisted proteins based on their detection in normal tissue by the Human Protein Atlas[32] to prioritize surface proteins with limited overall expression in normal tissue (Figure 2C). Based on this data mining strategy, the top three TNBC-associated surface proteins were EFNA4, ALPP, and PLXNB3. Provided that both EFNA4 and ALPP have previously been implicated in the context of breast cancer,[48,49] PLXNB3, a cell surface *N*-glycoprotein belonging to the class B of the plexin family,[50−52] was selected as a candidate of interest for functional interrogation. In our data, PLXNB3 was detected with two *N*-glycopeptides (FSAPNTTLNHLALAPGR and IVCVT-SPAPNGTTGPVR) out of eight theoretical tryptic *N*-glycopeptides.

Publicly available immunohistochemistry (IHC) data from the Human Protein Atlas (Figure 2C) and global proteomics data from normal human tissues (Figure S2A) consistently indicated that PLXNB3 is a glycoprotein with limited expression in normal tissues,[32,33] making PLXNB3 an attractive candidate for novel targeted therapies. In specific, IHC shows that PLXNB3 expression is restricted to the central nervous system (Figure S2B);[32] mass spectrometric data show minimal PLXNB3 expression in the female and reproductive tract, peripheral nerves, heart, lung, and parts of the digestive system (Figure S2A).[33] Notably, *N*-glycoproteomics also showed low PLXNB3 expression in only one of our five NC cells with undetectable levels in the other four NC lines, while PLXNB3 was highly expressed in five of the six TNBC cell lines investigated (Figure 2D). Finally, we interrogated PLXNB3 expression in breast cancer patients and found that high PLXNB3 mRNA expression in the TCGA RNA-seq data set[35] was associated with worse overall survival for breast cancer patients (Figure 2E), and similar trends were observed in the METABRIC data set[36] (Figure S2C). Increased PLXNB3 mRNA expression was also observed in moderately and poorly differentiated breast tumors compared to well-differentiated tumors.[53]

Moreover, prior reports indicated that PLXNB3 expression inversely correlated with estrogen receptor (ER)α expression.[53] Indeed, PLXNB3 expression in patients participating in the TCGA study was highest in basal-like and HER2+ breast cancer (data not shown) subtypes unlikely to express ERα[54] and historically associated with poor overall survival,[2] thus providing further evidence that PLXNB3 overexpression is associated with more aggressive breast tumors. Altogether, PLXNB3 is a previously undescribed TNBC-associated protein with low expression in normal tissue and prognostic value in larger patient cohorts.

Knockdown of PLXNB3 Impairs Cancer Cell Growth In Vitro

To clarify PLXNB3 function in tumor pathobiology, we proceeded to knockdown (KD) PLXNB3 in TNBC cells in vitro (Figure S3A,B). Suppression of PLXNB3 significantly impaired 2D cancer cell growth compared to nontreated (NT), mock, and scrambled (Scr) controls (Figure 3A). Notably, PLXNB3-negative cancer (HCC1937) and normal mammary epithelium (MCF10A) cell lines both were not impacted by transfection with anti-PLXNB3 siRNAs (Figure 3A). Moreover, PLXNB3 KD negatively impacted TNBC cell ability to establish colonies from single cells (Figures 3B and S3C), while, in contrast, colony forming ability in the PLXNB3-negative cell line HCC1937 was again not affected by transfection with siRNAs. Since two-dimensional assays do not recapitulate the complex growth and oxygenation patterns in 3D tissues,[55] we furthermore grew the cancer cells on low adhesion plates and embedded them in Matrigel to evaluate the impact of PLXNB3 KD on 3D cancer cell growth. Spheroid growth was negatively impacted by PLXNB3 KD in MDA-MB157 TNBC cells when compared to Scr, mock, and NT controls, while the PLXNB3-negative cell line HCC1937 demonstrated no growth impairment upon transfection with siRNA (Figure S3D). In sum, suppression of PLXNB3 impairs the growth of TNBC cells.

PLXNB3 Downregulation Reduces TNBC Cell Migration and Invasion

Several reports indicate that PLXNB3 signaling is involved in actin cytoskeleton remodeling and cell motility.[56−58] We therefore investigated if PLXNB3 downregulation impacts TNBC cell migration. Cancer cells grown as spheroids can invade the extracellular matrix in which they are embedded.[55] We observed that MDA-MB157 and HCC1937 cells grown as spheroids regularly invaded the adjacent extracellular matrix (Figure S3D). We quantified the number of Matrigel-invading cells (using ImageJ) and observed that PLXNB3 KD reduced MDA-MB157 cells' ability to invade the adjacent ECM compared to Scr, mock, and NT controls; the ability of the

https://doi.org/10.1021/acs.jproteome.2c00332
J. Proteome Res. 2022, 21, 2224−2236

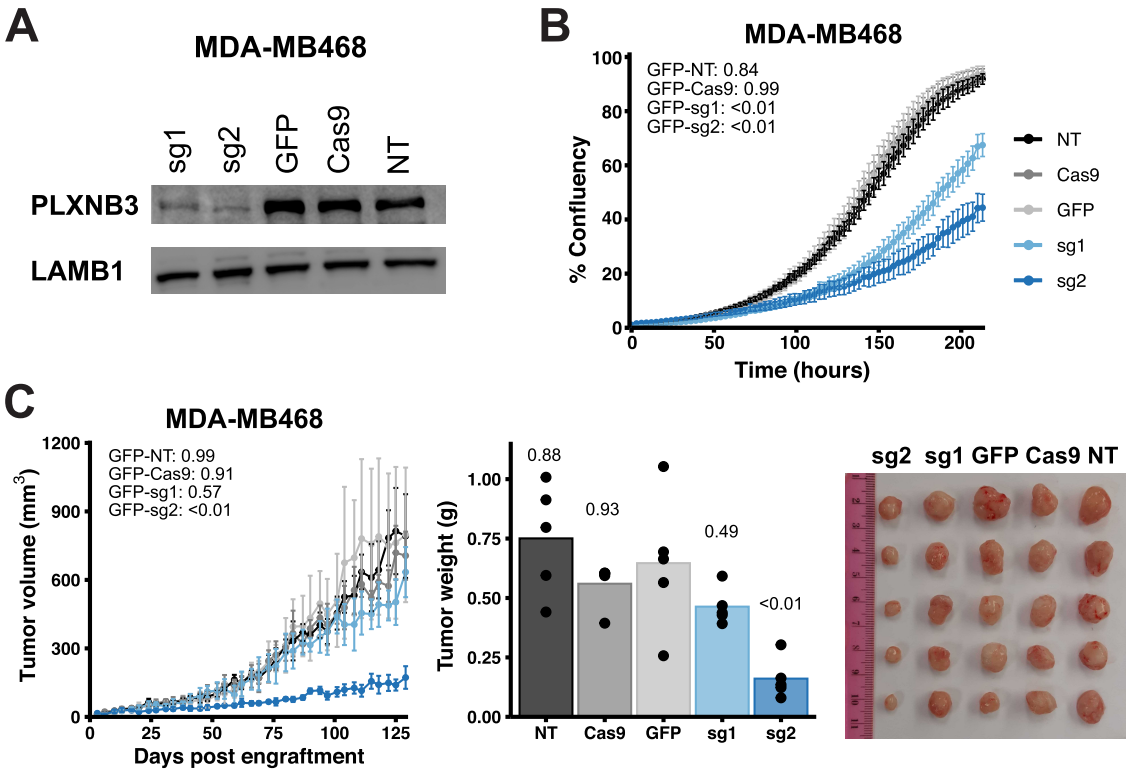

Figure 4. CRISPR-induced downregulation of pLXNB3 negatively impacts TNBC growth in vitro and in vivo. (A) CRISPR KD (polyclonal population) in MDA-MB468 cells results in reduced expression of the PLXNB3 protein compared to control conditions as determined by western blotting (sg1 and sg2: guide RNAs targeting PLXNB3; GFP: cells transfected with a guide RNA against GFP; Cas9: cells transfected with a vector only containing Cas9; NT: nontreated cells). (B) PLXNB3 KD using CRISPR-Cas9 negatively impacts 2D cancer cell growth as determined by the growth curve assay compared to sgGFP, Cas9, and NT controls. Average values with standard deviation are represented (n = 6). P-values from Tukey's multiple comparisons test against sgGFP control are reported. (C) PLXNB3 KD using CRISPR-Cas9 negatively impacts the in vivo tumor growth ability of MDA-MB468 cells (polyclonal population) grown subcutaneously in NSG mice. Left to right: Tumor volume (average values with standard deviation, n = 5), tumor weight, and picture of tumors at sacrifice. P-values from Tukey's multiple comparison test against sgGFP control are reported. See also Figure S4.

PLXNB3-negative cell line HCC1937 to invade Matrigel remained unaffected by the siRNA treatment (Figure 3C). We next interrogated if PLXNB3 downregulation can impede cancer cell migration in a chemoattractant gradient. Cells were seeded in an FBS-free medium on top of Transwell membranes and were allowed to migrate toward FBS-containing media over 18 h. Once again, PLXNB3 downregulation reduced migration of TNBC cells but not of the PLXNB3-negative cell line HCC1937 (Figure S3E), altogether indicating that PLXNB3 is involved in TNBC malignant cell migration and invasion.

PLXNB3 Downregulation Induces Apoptosis Markers in TNBC Cells

Since PLXNB3 downregulation impaired cancer cell growth, migration, and invasion, we proceeded to query the potential role of PLXNB3 in apoptosis in TNBC cells. First, we evaluated protein levels of the apoptosis markers cleaved caspase-3 and cleaved caspase-7[59] in whole cell lysates of PLXNB3 KD versus control cells. Cells were harvested and lysed after 24, 48, and 72 h following treatment or seeding (for NT controls). Total caspase-3 and caspase-7 levels relative to LAMB1 (loading control) remained unaltered in the cell lines across the different experimental conditions. Yet, following PLXNB3 downregulation in TNBC cells, cleaved caspase-3 and cleaved caspase-7 protein levels increased after 48 and 72 h (Figure S3A). Notably, an increase in cleaved caspase-3 and cleaved caspase-7 levels was detectable also in the control cell line HCC1937 (PLXNB3-negative), but at significantly lower levels (Figure S3A). No significant elevation of cleaved caspase-3 and cleaved caspase-7 levels could be detected in the Scr, mock, or NT controls (Figure S3A). Altogether, PLXNB3 downregulation induced apoptosis markers in TNBC cells. We therefore conclude that PLXNB3 KD in TNBC cells negatively impacts cancer cell growth and cancer cell viability.

CRISPR-Induced PLXNB3 Downregulation Negatively Impacts In Vivo Cancer Cell Growth

To evaluate the effects of PLXNB3 KD in vivo, we employed CRISPR-Cas9 technology in MDA-MB468 cells. Immunoblotting in MDA-MB468 cells demonstrated a significant reduction in PLXNB3 protein levels using two independent PLXNB3 targeting single guide RNAs (sgRNA, Figure 4A). Consistent with our findings using siRNA KD (Figure 3A), CRISPR-mediated downregulation of PLXNB3 reduced 2D cell growth (Figure 4B) as well as 3D spheroid growth (n = 3) (Figure S4A). Molecular perturbation of protein expression via two independent technologies (siRNA and CRISPR-Cas9) suggests the robustness of our observed phenotypes. Furthermore, we also detected the expected significant elevation of cleaved caspase-3 and cleaved caspase-7 levels in MDA-MB468 CRISPR-edited cells (Figure S4B) compared to the controls, suggesting the same induction of cell death pathways we had observed as a result of siRNA KD of PLXNB3. We then proceeded to determine the effects of PLXNB3 downregulation

https://doi.org/10.1021/acs.jproteome.2c00332
J. Proteome Res. 2022, 21, 2224−2236

on TNBC growth in vivo and subcutaneously implanted 1×10^6 CRISPR-edited MDA-MB468 cells in female NSG mice, along with the respective controls (sgGFP, Cas9, nontreated parental MDA-MB468 cells). The sg2-PLXNB3 polyclonal population growth was severely impaired in vivo (Figure 4C); similar to the in vitro growth assay (Figure 4B), the growth impairment in vivo was less pronounced for the sg1-PLXNB3 polyclonal population (28.3% reduction in tumor weight and 20% reduction in tumor volume compared to GFP at the endpoint but did not reach statistical significance). We hypothesize that the polyclonal nature of these PLXNB3 CRISPR-edited MDA-MB468 populations impacted the in vivo growth pattern and partially CRISPR-edited cells eventually outcompeted MDA-MB468 cells with stronger PLXNB3 depletion. No monoclonal PLXNB3 CRISPR-edited KO cells could be isolated, indicating that PLXNB3 loss is detrimental in TNBC cells already expressing the protein.

Interestingly, it has been previously reported that PLXNB3 KD in pancreatic cancer negatively impacted cancer tumor growth in vivo while increasing cancer cell migration and metastasis.[58] We therefore conclude that PLXNB3's role is tumor-dependent and may be influenced by ligand interaction. The partner of interaction for PLXNB3 in TNBC is currently unknown. SEMA5A and, to a lesser degree, SEMA4A are the reported ligands of PLXNB3.[60] However, mining of TCGA transcriptomic data shows that PLXNB3 expression inversely correlates with SEMA5A expression and positively correlates with SEMA4A expression in breast cancer, thereby suggesting that PLXNB3 does not signal via its canonical partner of interaction (i.e., SEMA5A) in TNBC. In our data set, only one cell line (MDA-MB157) was positive for SEMA5A, and no cell line was positive for SEMA4A. We cannot exclude a yet unknown partner of interaction for PLXNB3. Further studies will need to be conducted to identify PLXNB3 putative ligands and signaling pathways activated in TNBC cells.

CONCLUSIONS

TNBC is a heterogeneous disease[61] that afflicts 10−20% of breast cancer patients.[3,62] Although TNBC is one of the most sensitive tumors to standard chemotherapy,[63,64] the scarcity of targeted adjuvant therapies is correlated with early recurrence and poor overall survival of TNBC patients. As a result, TNBC is characterized by higher mortality rates compared to hormone receptor and/or HER2-positive breast tumors, for which the advent of targeted therapies has led to increased overall survival.[2] Our *N*-glycocapture approach led to the identification of PLXNB3 as a protein overexpressed in aggressive breast cancer compared to normal tissues. PLXNB3 downregulation negatively impacted TNBC cell growth, cell viability, and cell migration in vitro. Our report, the first one to interrogate the function of this poorly studied cell surface protein in breast cancer, therefore suggests PLXNB3 is involved in breast cancer tumorigenesis and could constitute a potential target of interest for novel therapies in this malignancy. Furthermore, our comprehensive TNBC *N*-glycoproteome list can be used for further data mining and identification of putative TNBC therapeutic targets. A limitation of this study is that though our simple *N*-glycocapture approach enriched for cell surface proteins, we do not directly measure protein expression at the cell surface. Although we leveraged a bioinformatics surface prediction tool to prioritize high-confidence cell surface proteins, the use of an alternative glycoproteomic approach, cell surface capture,[65] would have provided experimental evidence of surface localization. Additionally, as our *N*-glycoproteomic method only uses *N*-linked glycans as a tag for the isolation of *N*-glycosylated peptides, followed by detection and quantitation of enzymatically released peptides (i.e., formerly *N*-glycosylated peptides), it is possible that glycosylation heterogeneity may affect protein quantification. Since our *N*-glycocapture approach does not provide structural glycan information, avenues for future research include characterizing intact glycopeptide differences in TNBCs and using site-directed mutagenesis to investigate the role of *N*-glycosylation on PLXNB3 function. Additional limitations that we are keen to interrogate in the future are direct detection in patient tissues using immunohistochemistry and a more detailed analysis of the signaling pathway downstream of PLXNB3 using our CRISPR-edited cell line models.

ASSOCIATED CONTENT

Supporting Information

The Supporting Information is available free of charge at https://pubs.acs.org/doi/10.1021/acs.jproteome.2c00332.

N-Glycoproteomics data (Table S1) (XLSX)

TNBC and NC gene ontology and KEGG terms (Table S2) (XLSX)

N-Glycoproteomic differences between TNBC and NC (Figure S1); PLXNB3 expression in publicly available data (Figure S2); siRNA knockdown of PLXNB3 negatively affects TNBC cell growth, viability, and migration in vitro (Figure S3); CRISPR-mediated knockdown of PLXNB3 negatively affects TNBC in vitro (Figure S4); and full western blot membranes (Figure S5) (PDF)

AUTHOR INFORMATION

Corresponding Author

Thomas Kislinger − *Princess Margaret Cancer Center, University Health Network, Toronto, Ontario M5G 1L7, Canada; Department of Medical Biophysics, University of Toronto, Toronto, Ontario M5G 1L7, Canada;* orcid.org/0000-0003-3525-5540; Email: thomas.kislinger@utoronto.ca

Authors

Laura Kuhlmann − *Princess Margaret Cancer Center, University Health Network, Toronto, Ontario M5G 1L7, Canada*

Meinusha Govindarajan − *Princess Margaret Cancer Center, University Health Network, Toronto, Ontario M5G 1L7, Canada; Department of Medical Biophysics, University of Toronto, Toronto, Ontario M5G 1L7, Canada*

Salvador Mejia-Guerrero − *Princess Margaret Cancer Center, University Health Network, Toronto, Ontario M5G 1L7, Canada*

Vladimir Ignatchenko − *Princess Margaret Cancer Center, University Health Network, Toronto, Ontario M5G 1L7, Canada*

Lydia Y. Liu − *Princess Margaret Cancer Center, University Health Network, Toronto, Ontario M5G 1L7, Canada; Department of Medical Biophysics, University of Toronto, Toronto, Ontario M5G 1L7, Canada;* orcid.org/0000-0001-6026-3169

https://doi.org/10.1021/acs.jproteome.2c00332
J. Proteome Res. 2022, 21, 2224−2236

Barbara T. Grünwald − *Princess Margaret Cancer Center, University Health Network, Toronto, Ontario M5G 1L7, Canada*

Jennifer Cruickshank − *Princess Margaret Cancer Center, University Health Network, Toronto, Ontario M5G 1L7, Canada*

Hal Berman − *Princess Margaret Cancer Center, University Health Network, Toronto, Ontario M5G 1L7, Canada; Department of Laboratory Medicine and Pathobiology, University of Toronto, Toronto, Ontario M5S 1A8, Canada*

Rama Khokha − *Princess Margaret Cancer Center, University Health Network, Toronto, Ontario M5G 1L7, Canada; Department of Medical Biophysics, University of Toronto, Toronto, Ontario M5G 1L7, Canada*

Complete contact information is available at: https://pubs.acs.org/10.1021/acs.jproteome.2c00332

Author Contributions

[‖]L.K. and M.G. contributed equally. L.K. and T.K. initially designed the study with contributions from all authors. J.C. and H.B. provided reagents. L.K., M.G., S.M.-G., V.I., L.Y.L., and B.G. performed the experiments. L.K. and M.G. performed analysis and data interpretation. L.K., M.G., and T.K. wrote the manuscript. All authors edited and reviewed the manuscript. R.K. and T.K. supervised this work.

Notes

The authors declare no competing financial interest.

■ ACKNOWLEDGMENTS

This work was funded through a CCS Innovation Grant (705758). L.K. was partially supported by a George Knudson and Helena Lam postdoctoral fellowship. M.G. was supported by an OGS Graduate student fellowship, a Kristi Piia CALLUM Memorial Fellowship in Ovarian Cancer Research, and an MBP Excellence OSOTF award. This research was funded in part by the Ontario Ministry of Health and Long-Term Care. The authors thank Dr. Ankit Sinha, Mr. Andrew Macklin, and Dr. Deborah Ng for technical assistance.

■ REFERENCES

(1) Lebert, J. M.; Lester, R.; Powell, E.; Seal, M.; McCarthy, J. Advances in the systemic treatment of triple-negative breast cancer. *Curr. Oncol.* **2018**, *25*, 142−150.

(2) Howlader, N.; Cronin, K. A.; Kurian, A. W.; Andridge, R. Differences in Breast Cancer Survival by Molecular Subtypes in the United States. *Cancer Epidemiol., Biomarkers Prev.* **2018**, *27*, 619−626.

(3) Lyons, T. G. Targeted Therapies for Triple-Negative Breast Cancer. *Curr. Treat. Options Oncol.* **2019**, *20*, 82.

(4) Lee, C. N.; Heidbrink, J. L.; McKinnon, K.; Bushman, V.; Olsen, H.; FitzHugh, W.; Li, A.; Van Orden, K.; He, T.; Ruben, S. M.; Moore, P. A. RNA interference characterization of proteins discovered by proteomic analysis of pancreatic cancer reveals function in cell growth and survival. *Pancreas* **2012**, *41*, 84−94.

(5) Overington, J. P.; Al-Lazikani, B.; Hopkins, A. L. How many drug targets are there? *Nat. Rev. Drug Discovery* **2006**, *5*, 993−996.

(6) Jiang, J.; Yuan, J.; Hu, Z.; Zhang, Y.; Zhang, T.; Xu, M.; Long, M.; Fan, Y.; Tanyi, J. L.; Montone, K. T.; et al. Systematic illumination of druggable genes in cancer genomes. *CellReports* **2022**, *38*, No. 110400.

(7) Elschenbroich, S.; Kim, Y.; Medin, J. A.; Kislinger, T. Isolation of cell surface proteins for mass spectrometry-based proteomics. *Expert Rev. Proteomics* **2010**, *7*, 141−154.

(8) Kuhlmann, L.; Cummins, E.; Samudio, I.; Kislinger, T. Cell-surface proteomics for the identification of novel therapeutic targets in cancer. *Expert Rev. Proteomics* **2018**, *15*, 259−275.

(9) Waas, M.; Littrell, J.; Gundry, R. L. CIRFESS: An Interactive Resource for Querying the Set of Theoretically Detectable Peptides for Cell Surface and Extracellular Enrichment Proteomic Studies. *J. Am. Soc. Mass Spectrom.* **2020**, *31*, 1389−1397.

(10) Apweiler, R. On the frequency of protein glycosylation, as deduced from analysis of the SWISS-PROT database. *Biochim. Biophys. Acta* **1999**, *1473*, 4−8.

(11) Gahmberg, C. G.; Tolvanen, M. Why mammalian cell surface proteins are glycoproteins. *Trends Biochem. Sci.* **1996**, *21*, 308−311.

(12) Pinho, S. S.; Reis, C. A. Glycosylation in cancer: mechanisms and clinical implications. *Nat. Rev. Cancer* **2015**, *15*, 540−555.

(13) Bausch-Fluck, D.; Hofmann, A.; Bock, T.; Frei, A. P.; Cerciello, F.; Jacobs, A.; Moest, H.; Omasits, U.; Gundry, R. L.; Yoon, C.; et al. A Mass Spectrometric-Derived Cell Surface Protein Atlas. *PLoS One* **2015**, *10*, e0121314.

(14) Hofmann, A.; Thiesler, T.; Gerrits, B.; Behnke, S.; Sobotzki, N.; Omasits, U.; Bausch-Fluck, D.; Bock, T.; Aebersold, R.; Moch, H.; et al. Surfaceome of classical Hodgkin and non-Hodgkin lymphoma. *Proteomics: Clin. Appl.* **2015**, *9*, 661−670.

(15) Martinko, A. J.; Truillet, C.; Julien, O.; Diaz, J. E.; Horlbeck, M. A.; Whiteley, G.; Blonder, J.; Weissman, J. S.; Bandyopadhyay, S.; Evans, M. J.; Wells, J. A. Targeting RAS-driven human cancer cells with antibodies to upregulated and essential cell-surface proteins. *eLife* **2018**, *7*, No. e31098.

(16) Wei, J.; Leung, K.; Truillet, C.; Ruggero, D.; Wells, J. A.; Evans, M. J. Profiling the Surfaceome Identifies Therapeutic Targets for Cells with Hyperactive mTORC1 Signaling. *Mol. Cell Proteomics* **2020**, *19*, 294−307.

(17) Chen, W.; Mou, K. Y.; Paige, S.; Aggarwal, R.; Leung, K. K.; Wells, J. A. Large remodeling of the Myc-induced cell surface proteome in B cells and prostate cells creates new opportunities for immunotherapy. *Proc. Natl. Acad. Sci. U.S.A.* **2021**, *118*, No. e2018861118.

(18) Leung, K. K.; Wilson, G. M.; Kirkemo, L. L.; Riley, N. M.; Coon, J. J.; Wells, J. A. Broad and thematic remodeling of the surfaceome and glycoproteome on isogenic cells transformed with driving proliferative oncogenes. *Proc. Natl. Acad. Sci. U.S.A.* **2020**, *117*, 7764−7775.

(19) Kläsener, K.; Jellusova, J.; Andrieux, G.; Salzer, U.; Böhler, C.; Steiner, S. N.; Albinus, J. B.; Cavallari, M.; Süß, B.; Voll, R. E.; et al. CD20 as a gatekeeper of the resting state of human B cells. *Proc. Natl. Acad. Sci. U.S.A.* **2021**, *118*, No. e2021342118.

(20) van Oostrum, M.; Campbell, B.; Seng, C.; Müller, M.; Tom Dieck, S.; Hammer, J.; Pedrioli, P. G. A.; Földy, C.; Tyagarajan, S. K.; Wollscheid, B. Surfaceome dynamics reveal proteostasis-independent reorganization of neuronal surface proteins during development and synaptic plasticity. *Nat. Commun.* **2020**, *11*, No. 4990.

(21) van Oostrum, M.; Müller, M.; Klein, F.; Bruderer, R.; Zhang, H.; Pedrioli, P. G. A.; Reiter, L.; Tsapogas, P.; Rolink, A.; Wollscheid, B. Classification of mouse B cell types using surfaceome proteotype maps. *Nat. Commun.* **2019**, *10*, No. 5734.

(22) Haverland, N. A.; Waas, M.; Ntai, I.; Keppel, T.; Gundry, R. L.; Kelleher, N. L. Cell Surface Proteomics of N-Linked Glycoproteins for Typing of Human Lymphocytes. *Proteomics* **2017**, *17*, No. 1700156.

(23) Mallanna, S. K.; Cayo, M. A.; Twaroski, K.; Gundry, R. L.; Duncan, S. A. Mapping the Cell-Surface N-Glycoproteome of Human Hepatocytes Reveals Markers for Selecting a Homogeneous Population of iPSC-Derived Hepatocytes. *Stem Cell Rep.* **2016**, *7*, 543−556.

(24) Mallanna, S. K.; Waas, M.; Duncan, S. A.; Gundry, R. L. N-glycoprotein surfaceome of human induced pluripotent stem cell derived hepatic endoderm. *Proteomics* **2017**, *17*, No. 1600397.

(25) Poon, E. N.-Y.; Luo, X.-L.; Webb, S. E.; Yan, B.; Zhao, R.; Wu, S. C. M.; Yang, Y.; Zhang, P.; Bai, H.; Shao, J.; et al. The cell surface marker CD36 selectively identifies matured, mitochondria-rich hPSC-cardiomyocytes. *Cell Res.* **2020**, *30*, 626−629.

(26) Shakiba, N.; White, C. A.; Lipsitz, Y. Y.; Yachie-Kinoshita, A.; Tonge, P. D.; Hussein, S. M. I.; Puri, M. C.; Elbaz, J.; Morrissey-Scoot, J.; Li, M.; et al. CD24 tracks divergent pluripotent states in mouse and human cells. *Nat. Commun.* **2015**, *6*, No. 7329.

(27) Yoon, C.; Song, H.; Yin, T.; Bausch-Fluck, D.; Frei, A. P.; Kattman, S.; Dubois, N.; Witty, A. D.; Hewel, J. A.; Guo, H.; et al. FZD4 Marks Lateral Plate Mesoderm and Signals with NORRIN to Increase Cardiomyocyte Induction from Pluripotent Stem Cell-Derived Cardiac Progenitors. *Stem Cell Rep.* **2018**, *10*, 87−100.
(28) Cogger, K. F.; Sinha, A.; Sarangi, F.; McGaugh, E. C.; Saunders, D.; Dorrell, C.; Mejia-Guerrero, S.; Aghazadeh, Y.; Rourke, J. L.; Screaton, R. A.; et al. Glycoprotein 2 is a specific cell surface marker of human pancreatic progenitors. *Nat. Commun.* **2017**, *8*, No. 331.
(29) Sinha, A.; Hussain, A.; Ignatchenko, V.; Ignatchenko, A.; Tang, K. H.; Ho, V. W. H.; Neel, B. G.; Clarke, B.; Bernardini, M. Q.; Ailles, L.; Kislinger, T. N-Glycoproteomics of Patient-Derived Xenografts: A Strategy to Discover Tumor-Associated Proteins in High-Grade Serous Ovarian Cancer. *Cell Syst.* **2019**, *8*, 345−351.e4.
(30) Kislinger, T.; Rahman, K.; Radulovic, D.; Cox, B.; Rossant, J.; Emili, A. PRISM, a generic large scale proteomic investigation strategy for mammals. *Mol. Cell. Proteomics* **2003**, *2*, 96−106.
(31) Waas, M.; Snarrenberg, S. T.; Littrell, J.; Jones Lipinski, R. A.; Hansen, P. A.; Corbett, J. A.; Gundry, R. L. SurfaceGenie: a web-based application for prioritizing cell-type-specific marker candidates. *Bioinformatics* **2020**, *36*, 3447−3456.
(32) Uhlén, M.; Fagerberg, L.; Hallström, B. M.; Lindskog, C.; Oksvold, P.; Mardinoglu, A.; Sivertsson, Å.; Kampf, C.; Sjöstedt, E.; Asplund, A.; et al. Tissue-based map of the human proteome. *Science* **2015**, *347*, No. 1260419.
(33) Jiang, L.; Wang, M.; Lin, S.; Jian, R.; Li, X.; Chan, J.; Dong, G.; Fang, H.; Robinson, A. E.; Consortium, G.; et al. A Quantitative Proteome Map of the Human Body. *Cell* **2020**, *183*, 269−283.e19.
(34) Reimand, J.; Kull, M.; Peterson, H.; Hansen, J.; Vilo, J. g:Profiler−a web-based toolset for functional profiling of gene lists from large-scale experiments. *Nucleic Acids Res.* **2007**, *35*, W193−W200.
(35) Cancer Genome Atlas Network. Comprehensive molecular portraits of human breast tumours. *Nature* **2012**, *490*, 61−70.
(36) Curtis, C.; Shah, S. P.; Chin, S.-F.; Turashvili, G.; Rueda, O. M.; Dunning, M. J.; Speed, D.; Lynch, A. G.; Samarajiwa, S.; Yuan, Y.; et al. The genomic and transcriptomic architecture of 2,000 breast tumours reveals novel subgroups. *Nature* **2012**, *486*, 346−352.
(37) P'ng, C.; Green, J.; Chong, L. C.; Waggott, D.; Prokopec, S. D.; Shamsi, M.; Nguyen, F.; Mak, D. Y. F.; Lam, F.; Albuquerque, M. A.; et al. BPG: Seamless, automated and interactive visualization of scientific data. *BMC Bioinf.* **2019**, *20*, 42.
(38) Ran, F. A.; Hsu, P. D.; Wright, J.; Agarwala, V.; Scott, D. A.; Zhang, F. Genome engineering using the CRISPR-Cas9 system. *Nat. Protoc.* **2013**, *8*, 2281−2308.
(39) Hart, T.; Tong, A. H. Y.; Chan, K.; Van Leeuwen, J.; Seetharaman, A.; Aregger, M.; Chandrashekhar, M.; Hustedt, N.; Seth, S.; Noonan, A.; et al. Evaluation and Design of Genome-Wide CRISPR/SpCas9 Knockout Screens. *G3 Genes|Genomes|Genetics* **2017**, *7*, 2719−2727.
(40) Thu, K. L.; Silvester, J.; Elliott, M. J.; Ba-Alawi, W.; Duncan, M. H.; Elia, A. C.; Mer, A. S.; Smirnov, P.; Safikhani, Z.; Haibe-Kains, B.; et al. Disruption of the anaphase-promoting complex confers resistance to TTK inhibitors in triple-negative breast cancer. *Proc. Natl. Acad. Sci. U.S.A.* **2018**, *115*, E1570−E1577.
(41) Tian, Y.; Zhou, Y.; Elliott, S.; Aebersold, R.; Zhang, H. Solid-phase extraction of N-linked glycopeptides. *Nat. Protoc.* **2007**, *2*, 334−339.
(42) Alkhatib, H.; Rubinstein, A. M.; Vasudevan, S.; Flashner-Abramson, E.; Stefansky, S.; Oguche, S.; Peretz-Yablonsky, T.; Granit, A.; Granot, Z.; Ben-Porath, I.et al.*Mapping Cellular Subpopulations Within Triple Negative Breast Cancer Tumors Provides a Tool for Cancer Sensitization to Radiotherapy*, bioRxiv; 2021 DOI: 10.1101/2021.01.07.425553.
(43) da Silva, J. L.; Cardoso Nunes, N. C.; Izetti, P.; de Mesquita, G. G.; de Melo, A. C. Triple negative breast cancer: A thorough review of biomarkers. *Crit. Rev. Oncol. Hematol.* **2020**, *145*, No. 102855.
(44) Lawrence, R. T.; Perez, E. M.; Hernández, D.; Miller, C. P.; Haas, K. M.; Irie, H. Y.; Lee, S.-I.; Blau, C. A.; Villén, J. The proteomic landscape of triple-negative breast cancer. *Cell Rep.* **2015**, *11*, 630−644.
(45) Lehmann, B. D.; Pietenpol, J. A.; Tan, A. R. Triple-negative breast cancer: molecular subtypes and new targets for therapy. *Am. Soc. Clin. Oncol. Educ. Book* **2015**, e31−e39.
(46) Wellenstein, M. D.; Coffelt, S. B.; Duits, D. E. M.; van Miltenburg, M. H.; Slagter, M.; de Rink, I.; Henneman, L.; Kas, S. M.; Prekovic, S.; Hau, C.-S.; et al. Loss of p53 triggers WNT-dependent systemic inflammation to drive breast cancer metastasis. *Nature* **2019**, *572*, 538−542.
(47) Huang, C.-K.; Chang, P.-H.; Kuo, W.-H.; Chen, C.-L.; Jeng, Y.-M.; Chang, K.-J.; Shew, J.-Y.; Hu, C.-M.; Lee, W.-H. Adipocytes promote malignant growth of breast tumours with monocarboxylate transporter 2 expression via β-hydroxybutyrate. *Nat. Commun.* **2017**, *8*, No. 14706.
(48) Damelin, M.; Bankovich, A.; Park, A.; Aguilar, J.; Anderson, W.; Santaguida, M.; Aujay, M.; Fong, S.; Khandke, K.; Pulito, V.; et al. Anti-EFNA4 Calicheamicin Conjugates Effectively Target Triple-Negative Breast and Ovarian Tumor-Initiating Cells to Result in Sustained Tumor Regressions. *Clin. Cancer Res.* **2015**, *21*, 4165−4173.
(49) Murad, R.; Avanes, A.; Ma, X.; Geng, S.; Mortazavi, A.; Momand, J. Transcriptome and chromatin landscape changes associated with trastuzumab resistance in HER2+ breast cancer cells. *Gene* **2021**, *799*, No. 145808.
(50) Zhang, X.; Shao, S.; Li, L. Characterization of Class-3 Semaphorin Receptors, Neuropilins and Plexins, as Therapeutic Targets in a Pan-Cancer Study. *Cancers* **2020**, *12*, No. 1816.
(51) Artigiani, S.; Conrotto, P.; Fazzari, P.; Gilestro, G. F.; Barberis, D.; Giordano, S.; Comoglio, P. M.; Tamagnone, L. Plexin-B3 is a functional receptor for semaphorin 5A. *EMBO Rep.* **2004**, *5*, 710−714.
(52) Balakrishnan, A.; Penachioni, J. Y.; Lamba, S.; Bleeker, F. E.; Zanon, C.; Rodolfo, M.; Vallacchi, V.; Scarpa, A.; Felicioni, L.; Buck, M.; et al. Molecular profiling of the "plexinome" in melanoma and pancreatic cancer. *Hum. Mutat.* **2009**, *30*, 1167−1174.
(53) Malik, M. F. A.; Ye, L.; Jiang, W. G. Reduced expression of semaphorin 4D and plexin-B in breast cancer is associated with poorer prognosis and the potential linkage with oestrogen receptor. *Oncol. Rep.* **2015**, *34*, 1049−1057.
(54) Marotti, J. D.; Collins, L. C.; Hu, R.; Tamimi, R. M. Estrogen receptor-beta expression in invasive breast cancer in relation to molecular phenotype: results from the Nurses' Health Study. *Mod. Pathol.* **2010**, *23*, 197−204.
(55) Tevis, K. M.; Colson, Y. L.; Grinstaff, M. W. Embedded Spheroids as Models of the Cancer Microenvironment. *Adv. Biosyst.* **2017**, *1*, 1700083.
(56) Li, X.; Lee, A. Y. W. Semaphorin 5A and plexin-B3 inhibit human glioma cell motility through RhoGDIalpha-mediated inactivation of Rac1 GTPase. *J. Biol. Chem.* **2010**, *285*, 32436−32445.
(57) Li, X.; Law, J. W. S.; Lee, A. Y. W. Semaphorin 5A and plexin-B3 regulate human glioma cell motility and morphology through Rac1 and the actin cytoskeleton. *Oncogene* **2012**, *31*, 595−610.
(58) Saxena, S.; Prajapati, D. R.; Goel, P.; Tomar, B.; Hayashi, Y.; Atri, P.; Rachagani, S.; Grandgenett, P. M.; Hollingsworth, M. A.; Batra, S. K.; Singh, R. K. Plexin-B3 Regulates Cellular Motility, Invasiveness, and Metastasis in Pancreatic Cancer. *Cancers* **2021**, *13*, No. 818.
(59) Taddei, M. L.; Giannoni, E.; Fiaschi, T.; Chiarugi, P. Anoikis: an emerging hallmark in health and diseases. *J. Pathol.* **2012**, *226*, 380−393.
(60) Worzfeld, T.; Offermanns, S. Semaphorins and plexins as therapeutic targets. *Nat. Rev. Drug Discovery* **2014**, *13*, 603−621.
(61) Jézéquel, P.; Loussouarn, D.; Guérin-Charbonnel, C.; Campion, L.; Vanier, A.; Gouraud, W.; Lasla, H.; Guette, C.; Valo, I.; Verrièle, V.; Campone, M. Gene-expression molecular subtyping of triple-negative breast cancer tumours: importance of immune response. *Breast Cancer Res.* **2015**, *17*, No. 43.
(62) Vagia, E.; Mahalingam, D.; Cristofanilli, M. The Landscape of Targeted Therapies in TNBC. *Cancers* **2020**, *12*, No. 916.
(63) Carey, L. A.; Dees, E. C.; Sawyer, L.; Gatti, L.; Moore, D. T.; Collichio, F.; Ollila, D. W.; Sartor, C. I.; Graham, M. L.; Perou, C. M. The triple negative paradox: primary tumor chemosensitivity of breast cancer subtypes. *Clin. Cancer Res.* **2007**, *13*, 2329−2334.

(64) Mirzania, M. Approach to the Triple Negative Breast Cancer in New Drugs Area. *Int. J. Hematol. Oncol. Stem. Cell Res.* **2016**, *10*, 115−119.
(65) Wollscheid, B.; Bausch-Fluck, D.; Henderson, C.; O'Brien, R.; Bibel, M.; Schiess, R.; Aebersold, R.; Watts, J. D. Mass-spectrometric identification and relative quantification of N-linked cell surface glycoproteins. *Nat. Biotechnol.* **2009**, *27*, 378−386.

https://doi.org/10.1021/acs.jproteome.2c00332
J. Proteome Res. 2022, 21, 2224−2236